Calculation of Thrust and Drag Characteristics for Ship's Propulsion Mechanism of Weis-Fogh Type

Ki-Deok Ro*

School of Transport Vehicle Engineering · Institute of Marine Industry, Gyeongsang National University

The flow field of a ship's propulsion mechanism of Weis-Fogh type is studied by the discrete vortex method. The wing in a channel is approximated by a finite number of bound vortices, and free vortices representing the separated flow are introduced from the trailing edge of the wing. The time histories of the thrust, the drag, and the moment acting on the wing are calculated, including the unsteady force due to the change of strength of the bound vortices. These calculated values agree well with the experimental values. The flow field of this propulsion mechanism is numerically clarified.

Key Words : Hydraulic Machine, Numerical Analysis, Unsteady Flow, Separation, Fluid Force, Discrete Vortex Method, Ship Propulsion

1. Introduction

The Weis-Fogh mechanism is a unique, highly efficient lift generating mechanism which Weis-Fogh discovered by observing the hovering flight of small bees called Encarsia formosa, as shown in Fig. 1(a), having body lengths of about 1mm (Weis-Fogh, 1973 and Lighthill, 1973). Figure 1 (b) shows the principles of the motions. Here, the bee is able to remain hovering flight by moving its wings in a horizontal plane while holding the body upright. First, the wings clap from the dorsal side of the body revolving around their leading edge. Then, they open their wings from the state where the trailing edges are touching each other(fling), move in the horizontal plane while maintaining a fixed open angle(we define the fixed open angle as 1/2 of the angle formed by intersection of two wings in the second one of Fig. 1(b)). The wings change their moving direction and the open angle on the ventral side(flap) and then move back to the horizontal plane and clap touching their leading edges again. These motions are repeated. The lower picture of Fig. 1 (b) shows a 2-dimensional model of this movement.

Generally, wings in a still state need some distance in order to gain sufficient circulation

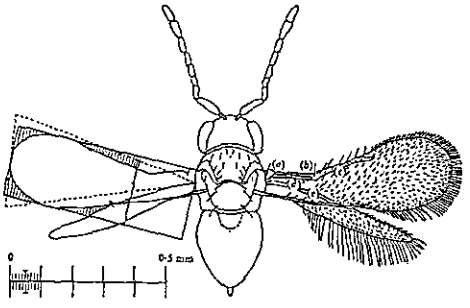

(a) Encarsia formosa

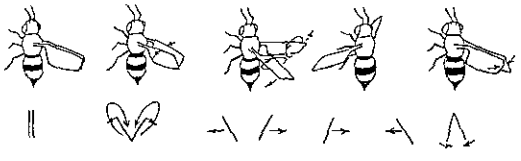

(b) Hovering flight

Fig. 1 Encarsia formosa and its hovering flight

* **E-mail** : rokid@gshp.gsnu.ac.kr
TEL : +82-55-640-3123 ; **FAX** : +82-55-640-3128
School of Transport Vehicle Engineering, Institute of Marine Industry, Gyeongsang National University,, 445, Inpyeong-dong, Tongyeong, Gyeongnam 650-160, Korea.(Manuscript **Received** November 3, 1999; **Revised** July 20, 2000)

around the wing for generating lift (Wargner effect). This is the case in airplane wings. However, in this mechanism, a pair of opposite circulations around wings is generated at the moment when the two wings open touching their trailing edge. This enables the wings to gain sufficient lift in spite of short stroke.

In the actual flight of Encarsia formosa, beating rate of the wings is about 400Hz. Here, the Reynolds number defined by the wing chord and mean velocity of the leading edge is approximately 30 and a lift coefficient of about 3~4(Weis-Fogh, 1973). Even when the area of hair surrounding the wing is included in calculating the wing surface area, the lift coefficient is higher than 1. 6(Lighthill, 1973). This value is much higher compared with that of steady wing for low Reynolds number and this means that the insect generates the lift force very efficiently.

For this reason, this mechanism has been attracting the attention of many fluid dynamics researchers(Maxworthy, 1979: Edwards, 1982: Spedding, 1986: and Ro, 1997). In addition, numerous attempts to apply this mechanism in the field of engineering have recently been very active (Furber and Ffowcs Williams, 1979 : Tsutahara and Kimura, 1987 : Tsutahara, Kimura and Ro, 1989 : Ro, 1993 : Tsutahara and Kimura, 1987 : and Tsutahara and Kimura, 1994).

Consequently, we have proposed a propulsion model where the 2-dimensional Weis-Fogh mechanism has been installed in a square channel. The experiments on the dynamic properties as well as working tests on the model ship were conducted. It was proved that the proposed propulsion mechanism could be potentially used as a ship propulsion (Tsutahara, Kimura and Ro, 1989). In addition, the visualization experiment through the hydrogen bubble technique with numerical simulation using the discrete vortex method enabled clear visualization of the unsteady flow field generated around the wings under the propulsion mechanism(Ro, 1993).

Continued from the last paper(Ro, 1993), this research is aimed at the time history of the thrust and drag coefficients of the Weis-Fogh type ship propulsion mechanism. This will be done through numerical calculation using the discrete vortex method.

2. Calculation Method

2.1 Analytical model

Figure 2 shows the analytical model of a Weis-Fogh type ship propulsion mechanism. This model is identical with the Ro's work(1993), but I would like to roughly go over it again for easier understanding.

A wing is installed in an square channel. When the point P which corresponds to the center axis of the wing is oscillated back and forth along the y-axis, the wing first opens about point P from the lower surface(opening stage). Then, maintaining an open angle α, the wing moves translationally in a parallel movement(translating stage), and finally rotates and closes on the upper surface(closing stage), by reciprocal motion of point P. It then executes an opening stage at the upper surface once more, moves translationally once again, and repeats the closing stage at the lower surface.

Originally, in the Weis-Fogh mechanism, circulation in the opposite direction of each other is formed at each wing, as a pair of flat-plate wings opens in touching their trailing edges. This is shown in Fig. 1(b). However, through the princi-

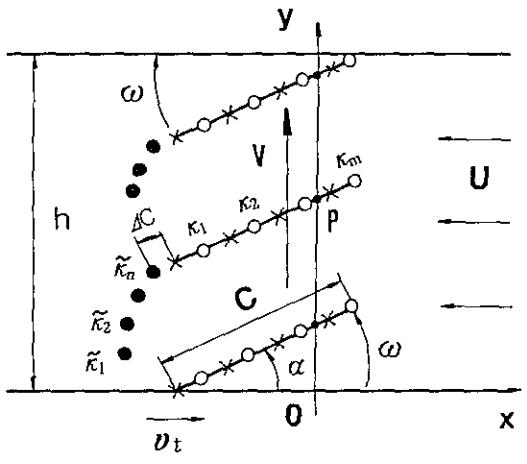

Fig. 2 An analytical model and time history of movement of the line element during a stroke within the channel

ple of mirror image, when channel walls are placed and the same motions above are executed by the single wing, shown in the analytical model of Fig. 2, the identical effects can be achieved as in the case of a pair of wings.

As shown in Fig. 2, the flow surrounding the wing is described here by equally placed finite number of bound vortices. The flow field is calculated at each time step as the wing is moved so as to simulate the wing motions described earlier. The complex potential $F(z)$ obtained from the whole flow field can be expressed as follows.

$$F(z)=i\sum_{j=1}^{m}x_j\left[\left\{\sinh\frac{\pi(z-z_j)}{2h}\right\}-\log\left\{\sinh\frac{\pi(z-\bar{z}_j)}{2h}\right\}\right]+i\sum_{l=1}^{n}\bar{x}_l\left[\log\left\{\sinh\frac{\pi(z-\bar{z}_l)}{2h}\right\}-\log\left\{\sinh\frac{\pi(z-\bar{\bar{z}}_l)}{2h}\right\}\right]-Uz \quad (1)$$

In the above equation, i is the imaginary number $\sqrt{-1}$, h is the width of a channel, $\bar{}$ is the complex conjugate, the U represents an uniform flow, while $x_j(j=1, 2, \ldots m)$ and z_j represent the strength and position of the bound vortices respectively. Also, $\bar{x}_l(l=1, 2, \ldots n)$ and $\bar{z}_l$ represent the strength and position of the free vortices respectively.

The conditions of the stream function, the conditions for the velocity, or the Kelvin's theorem were used in determining the strengths of the vortices at each time step(Ro, 1993). For example the detailed method at the opening stage is shown in Fig. 3. As point P moves in the direction of y-axis, the trailing edge of the wing which is adjacent to the wall surface moves in the direction of x-axis. The entire wing namely opens through revolving around the point P. The motion of wing at this stage can be separated into the motion that the wing opens around the trailing edge at an angular velocity of ω, and the motion that the whole wing translates in the direction of the x-axis at a velocity of v_t. Therefore the normal component of the velocity $\boldsymbol{v}\cdot\boldsymbol{n}$ in each motion, acting on the point a distance r away from the trailing edge when the open angle of the wing is α, is $r\omega$ and $v_t \sin\alpha$ respectively,

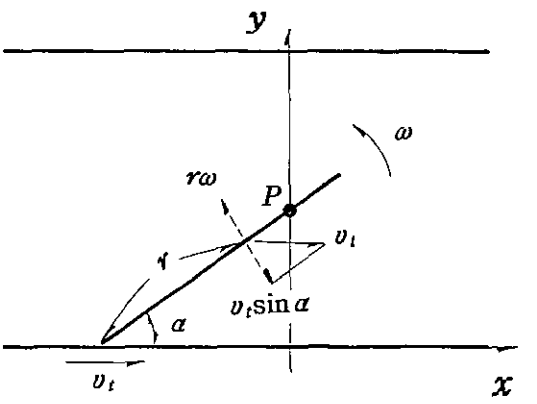

Fig. 3 Illustration for the boundary conditions

as shown in Fig. 3.

Also, recalling the definition of the stream function $\Psi=Im\{F(z)\}$, its equation at the control point, located at the centers between adjacent vortices, is calculated as follows.

$$\Psi=\int_0^r \boldsymbol{v}\cdot\boldsymbol{n}\,dr=v_t\sin\alpha\cdot r-\frac{1}{2}\omega r^2 \quad (2)$$

The boundary conditions for the translating stage and closing stage are calculated similarly. Detailed calculation methods are given by Ro (1993).

On the other hand, the free vortices representing the wake are generated at each time step Δt, at a location ΔC away from the trailing edge of the wing. Here, the Euler's equations are applied for calculating the motions of $\bar{z}_l$, the lth free vortex.

$$\bar{z}_l(t+\Delta t)=\bar{z}_l(t)+\bar{W}\cdot\Delta t$$
$$W=\frac{d}{dz}\left[F(z)-i\bar{x}_l\log\left\{\sinh\frac{\pi(z-\bar{z}_l)}{2h}\right\}\right] \quad (3)$$

where W represents the complex velocity induced by total bound and free vortices except $\bar{z}_l$ in the flow field.

2.2 The Force and moment acting on the wing

Let X, Y represent the x and y components of the force acting on the wing, shown in Fig. 2. The value of these components can be obtained by

contour integration of the pressure around the wing surface as follows.

$$X-iY=\frac{i\rho}{2}\oint_B\left(\frac{dF}{dz}\right)^2dz+i\rho\oint_B\frac{\partial\bar{F}}{\partial t}d\bar{z} \quad (4)$$

In the above equation ρ represents the density of the fluid while is the integral path of the wing surface. Also, $\coth\{\pi(z-z_j)/2h\}$ has its first extreme value at $z=z_j$ where the residue is $2h/\pi$. Therefore, the first term on the right hand side of Eq. (4) can be expressed as follows.

$$\begin{aligned}\frac{i\rho}{2}\oint_B\left(\frac{dF}{dz}\right)^2=&-\pi\rho\Bigg[\frac{\pi}{h}\sum_{j=1}^{m}x_j{}^2\coth\frac{\pi(z_j-\bar{z}_j)}{2h}-\frac{\pi}{2h}\sum_{j=1}^{m}x_j\\&\times\Bigg[\sum_{\substack{k=1\\k\neq j}}^{m}x_k\left\{\coth\frac{\pi(z_j-z_k)}{2h}-2\coth\frac{\pi(z_j-\bar{z}_k)}{2h}\right\}\Bigg]\\&-\frac{\pi}{h}\sum_{j=1}^{m}x_j\left\{\coth\frac{\pi(z_j-\tilde{z}_l)}{2h}\right.\\&\left.-\coth\frac{\pi(z_j-\bar{\tilde{z}}_l)}{2h}\right\}\Bigg]-2Ui\sum_{j=1}^{m}x_j\Bigg] \quad (5)\end{aligned}$$

The second term on the righthand side of Eq. (4) can be evaluated by a method which we proposed (Tsutahara, Kimura and Ro, 1989). It uses the assumption that the wing surface is the collective cuts of the logarithmic singularities. This is obtained by finding the argument difference between the upper and lower surfaces of the wing. Organizing all these into one equation results in the following.

$$\begin{aligned}i\rho\oint_B\frac{\partial\bar{F}}{\partial t}d\bar{z}=2i\pi\rho\Bigg[&\sum_{j=1}^{m}x_j\dot{\bar{z}}_j+e^{-i\alpha}\left\{\sum_{j=1}^{m}\left(\sum_{q=j}^{m}\dot{x}_q\right)\Delta r_j\right.\\&\left.+\frac{\tilde{x}_l{}^{new}}{\Delta t}\cdot C\right\}\Bigg] \quad (6)\end{aligned}$$

where

$$\dot{x}_j=\frac{x_j(t)-x_j(t-\Delta t)}{\Delta t} \quad (7)$$

denotes the time rate of the strength of the bound vortices.

In this equation. $\dot{\bar{z}}_j$ represents the complex velocity conjugate of the bound vortices and can be calculated easily from the velocity of the wing translation V. Also, α represents the open angle of the wing and $\tilde{x}_l{}^{new}$ is the strength of the free vortex which is newly generated at each time step while Δr_j is the infinitesimal distance between z_j and z_{j-1}.

In this case, to facilitate the calculation for M_p, the moment around point P in Fig. 2, the moment around the trailing edge M_t is obtained first and the results are used along with X, Y obtained from Eq. (4) to give the following formula.

$$\left.\begin{aligned}M_p&=M_t+Im\{(X-iY)(z_p-z_t)\}\\M_t&=-Re\left\{\frac{\rho}{2}\oint_B\left(\frac{dF}{dz}\right)^2(z-z_t)\,dz\right\}\\&\quad+e^{-2i\alpha}\rho\oint_B\frac{\partial\bar{F}}{\partial t}(\bar{z}-\bar{z}_t)\,d\bar{z}\end{aligned}\right] \quad (8)$$

In this equation Im and Re represent the imaginary and real components respectively while Z_p and Z_t each are the position of point P and the trailing edge of the wing which is expressed as $z=x+iy$.

On the other hand, M_t in the above equation, which is the moment around the trailing edge, can be obtained from the similar methods in calculating the force. Here we show only the simplified resultant equation.

$$\begin{aligned}M_t=&-Re\Bigg[i\pi\rho e^{i\alpha}\Bigg[\frac{\pi}{h}\sum_{j=1}^{m}x_j^2r_j\coth\frac{\pi(z_j-\bar{z}_j)}{h}\\&-\frac{\pi}{h}\sum_{j=1}^{m}x_jr_j\Bigg[\sum_{\substack{k=1\\k\neq j}}^{m}x_k\left\{\coth\frac{\pi(z_j-z_x)}{2h}\right.\\&\left.-2\coth\frac{\pi(z_j-\bar{z}_k)}{2h}\right\}\Bigg]-\frac{\pi}{h}\sum_{j=1}^{m}x_jr_j\Bigg[\sum_{l=1}^{n}\tilde{x}_l\\&\times\left\{\coth\frac{\pi(z_j-\tilde{z}_l)}{2h}-\coth\frac{\pi(z_j-\bar{\tilde{z}}_l)}{2h}\right\}\Bigg]\\&-2Ui\sum_{j=1}^{m}x_jr_j\Bigg]+2\pi\rho e^{i\alpha}\sum_{j=1}^{n}x_j\dot{\bar{z}}_jr_j\\&+\pi\rho\Bigg[\sum_{j=1}^{m}\left\{\left(\sum_{q=j}^{m}\dot{x}_q\right)+\frac{\tilde{x}_l{}^{new}}{\Delta t}\right\}(r_j^2-r_{j-1}^2)\\&+\frac{\tilde{x}_l{}^{new}}{\Delta t}(C^2-r_m^2)\Bigg]\Bigg] \quad (9)\end{aligned}$$

In the above equation, r_j is the distance from the trailing edge of the wing to z_j while r_m is the distance from z_1 to z_m.

2.3 Coefficients of properties

The thrust coefficient C_T and the drag coefficient C_D representing the dynamical properties of the propulsion mechanism can be calculated as follows. Assuming the thrust T as the component of force opposite to the x component of uniform flow U acting on the wing axis which is approximated as point P, the thrust T corresponds to X of Eq. (4). Assuming the drag D as the component of force opposite to the y component of the wing velocity V, the drag D corresponds to -Y of

Eq. (4).

However, the reaction force to the moment M_P around the wing axis must be put into consideration as drag during the opening and closing stages. In other words, if we define r_p as the distance from the trailing edge of the wing to point P, the reaction force at the wall surface during the opening stage equals $Y_W = M_P \cos\alpha / r_p$ when a counterclockwise moment is applied. Similarly, the reaction force during the closing stage equals $Y_w = M_P \cos\alpha / (C - r_p)$ when a clockwise moment is applied. This value is added to the drag force.

Since the calculations are done in 2-dimensions, if we take the unit length as the wing span, the thrust coefficient C_T and drag coefficient C_D acting on the wing axis can be calculated as follows.

$$C_T = \frac{X}{\frac{1}{2}\rho V^2 C} \tag{10}$$

$$C_D = \frac{-Y + Y_w}{\frac{1}{2}\rho V^2 C} \tag{11}$$

2.4 Parameter values in the calculations

As for the parameter values in calculations, the wing chord $C=1$, density of fluid $\rho=1$, movement velocity of wing axis $V=1$, width of water channel $h=4C$ and the distance from the trailing edge of the wing to the wing axis r_p is fixed at $r_p = 0.75$. The open angle α and the ratio between the movement velocity of the wing axis and the uniform flow V/U is appropriately changed in calculating the thrust coefficient C_T and the drag coefficient C_D. In addition, the number of bound vortices representing the wing is m=20, while the distance from the trailing edge of the wing to the insertion point of the free vortices is set as $\Delta C = 0.05C$.

There are two methods widely used in the discrete vortex method to insert the free vortex at a separation point; the first method is by assuming the insertion point near the vicinity of the separation point and then determining the strength of the vortex using the Kutta's conditions or the conditions for stream function, and the second method uses the boundary layer theory to get the strength of the vortex and then determines the insertion point using the Kutta's conditions.

In this experiment the former method was used for the calculations where ΔC was approximated as $0.02C \sim 0.08C$ which would not seriously affect the calculation results. Consequently, it agreed well with the empirical results. In accordance with the visualization experiments, the free vortices were generated once every time step at the trailing edge. Considering my last paper (Ro, 1993) there was no generation of vortices at the trailing edge in the opening stage because the edge was touched on the channel wall in this stage but only during the translating stage and the closing stage. Also, the time step Δt was set as $\Delta t = 0.1$ during the translating stage and as $\Delta t_0 = \Delta t \times r_p C$ and $\Delta t_c = \Delta t \times (1 - r_p) C$ during the opening and closing stages respectively. The results of the above procedure reveal these values of time steps that the distances moved by the leading or trailing edges are all equal during the entire stroke. The present work indicats that a total of 39 free vortices is generated each stroke in calculation.

3. Equipment

3.1 Driving system of the wing

In this experiment, the driving unit of a wing was assembled as an analytical model shown in Fig. 2, at which the measurements of the thrust and drag were taken by the degree of deformation of the strain gauge. In our previous experiments (Tsutahara and Kimura, 1987: and Tsutahara, Kimura and Ro, 1989), the values were measured by pulling the drive system at the speed of the uniform flow in a towing water tank. However, in this experiment they were measured by stabilizing the drive system in the circulating water tank idealized in my previous paper (Ro, 1993) and then streaming the uniform flow against the system.

A sketch of the driving system is shown in Fig. 4. The unit was built out of aluminium angle with a length of 500 mm, width of 650 mm and a height of 635 mm so as to match the size of the circulat-

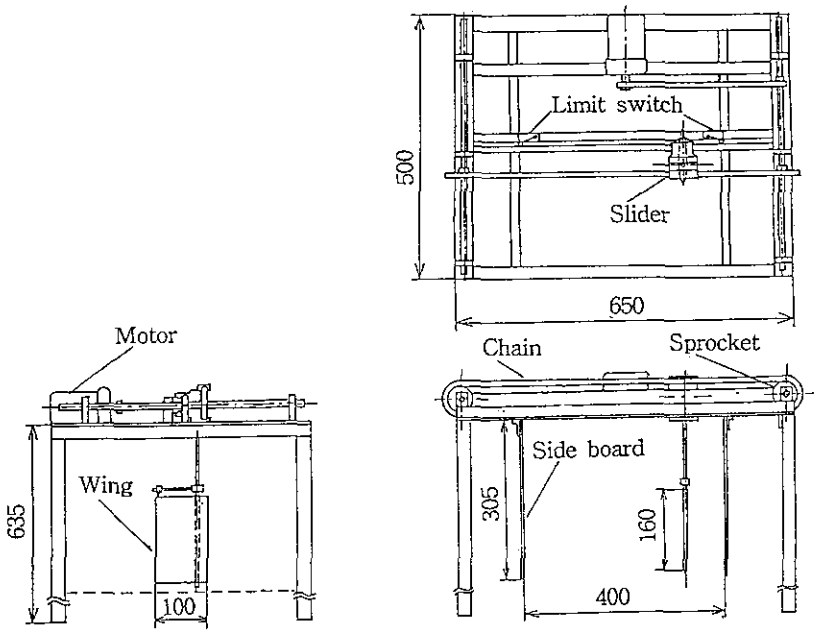

Fig. 4 Driving unit of the wing(unit : mm)

ing water tank explained in my last paper(Ro, 1993). The wing axis penetrating the wing was fixed to the slider which was fixed to a point of the chain. The power generated from the motor (DC 30W, sprocket attached) was relayed through the chain, operating axis, sprocket and slider to the wing. The reciprocating motion of the wing was made possible by use of the limit switches installed at both ends of the rail along with a relay circuit to control the motor in rotating forward or reverse.

The movement velocity of the wing was controlled by revolution speed of the motor. Also. a support perpendicular to the wing axis was installed where the length of the string connected from the support to the trailing edge of the wing would set the open angle α in Fig. 5. In the state where the wing was linked to the axis, the moment around the wing axis generated during the reciprocal motions functions to open the wing. In the closing stage, the leading edge of the wing hit the side board forcing the wing to close.

3.2 Measurement of the thrust and drag acting on the wing

The wing used in this experiment had a chord

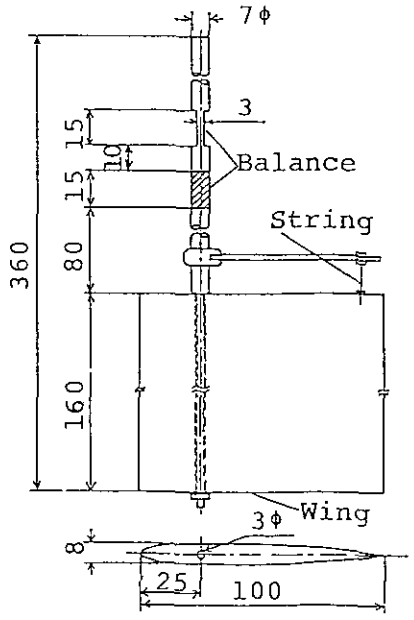

Fig. 5 Structure of the wing and shaft(unit : mm)

of 100 mm and a span of 160 mm as shown in Fig. 5. The hole where the axis was linked was located at a point 0.75C away from the trailing edge. In order to reduce the effect of inertia, the wing was made out of 8 mm thick light wood.

The driving unit was installed as the analytical

model shown in Fig. 2 so that the wing moved back and forth perpendicular to the uniform flow. The definition here on the thrust and drag were identical with the analytical model. The axis of the wing was made out of a 7 mm steel rod with the upper part cut evenly in order to facilitate measurement of the thrust and drag as shown in Fig. 5. Four strain gauges were attached to the balance of the axis. The thrust and drag measurements were done by deformation of these gauges. In this stage, the voltage waves generated from each channel (total 2) of these strain gauges would go through a bridge circuit, a strain amp, and then an AD converter to be input and then processed by a PC.

As for the experiment conditions, the channel width was fixed at h=400 mm and the open angle α ranged from 10° to 30° with interval 5°. At this stage, the time history measurements of the drag and thrust were taken at moderate variations of uniform flow U (U=0.16~0.31 m/sec) and wing speed V (V=0.12~0.36 m/sec).

4. Results and Discussions

Before proceeding with the calculated results of the dynamic properties, we shall observe Fig. 6 which displays the continuous flow pattern around the wing during a stroke, to visually prove the validity of this calculation method. Figure 6

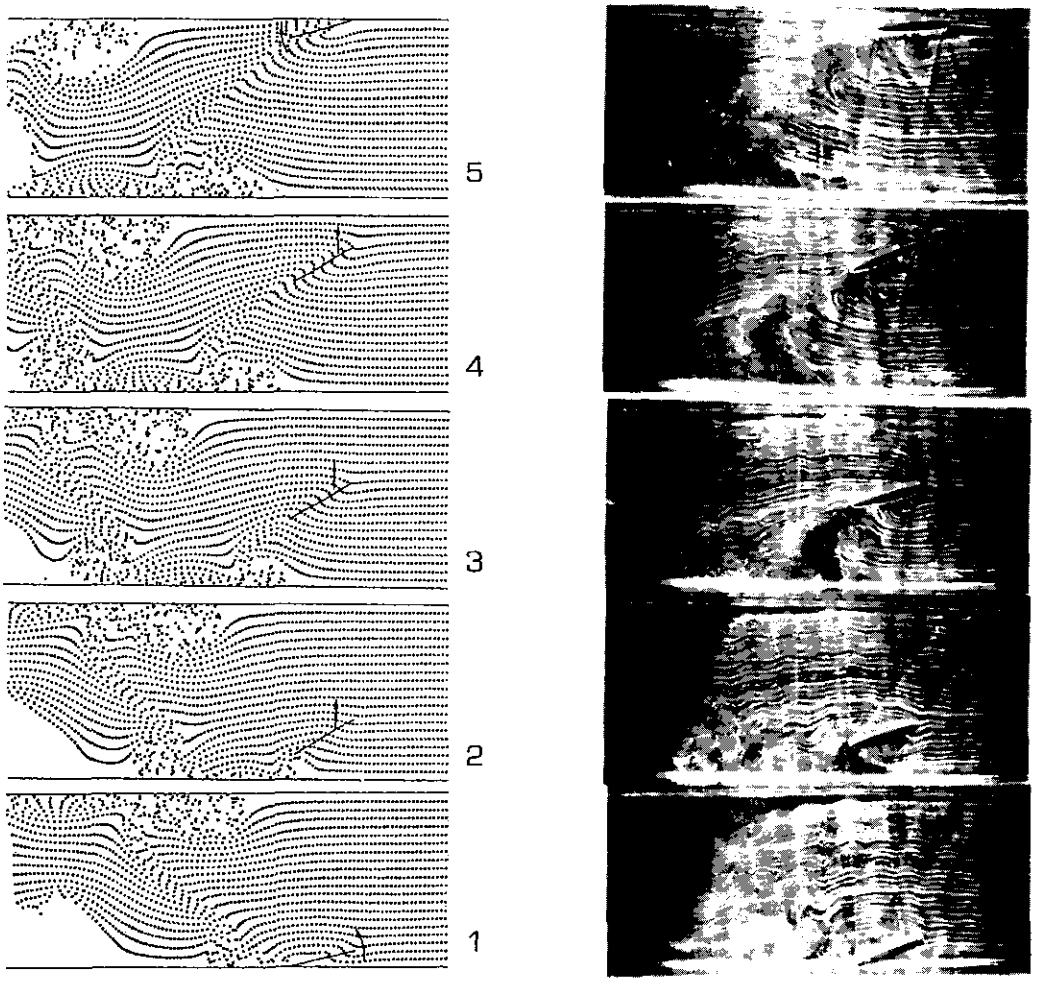

(a) Simulation (b) Photograph

Fig. 6 Flow pattern for one stroke of the wing(C=1, $h=2.5C$, $V/U=1.0$, $r_p=0.75C$, $\alpha=30°$)

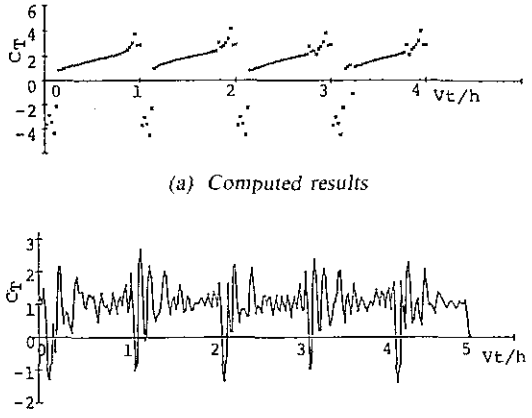

(a) Computed results

(b) Measured results

Fig. 7 Time variations for thrust coefficients($C=1$, $h=4C$, $V/U=1.0$, $r_p=0.75C$, $\alpha=30°$)

(a) is the numerical simulation result of the streak lines while Fig. 6(b) is a visualized picture taken using the hydrogen bubble method under the same conditions as Fig. 6(a). The hydrogen bubble method was explained in my last paper *(Ro, 1993)*. *Also in the figure, 1 represents the* opening stage, 2 to 4 the translating stages, and 5 the closing stage. The discontinuity of the streak lines seen in the vicinity of the trailing edge is due to the effects from the vortices generated at the trailing edge. In overall, the simulation results of the whole stage matches with the visualized picture.

The followings are the calculated results of the dynamic properties. Figure 7 shows the time history of the thrust coefficient C_T at $\alpha=30°$ and V/U=1.0. The horizontal axis in the figure represents the value that the moved distance of the wing axis is divided by the channel width. This value corresponds to the number of strokes. Figure 7(a) is the calculated result while Fig. 7 *(b) is the measured value taken under the same* conditions. The reason that the measured results have the large fluctuations is due to the surface wave generated by the movement of the wing, and particularly the larger fluctuations occurred in the early stage of each stroke is because the wing axis is instantaneously acted at the large force, due to the inertial force of the wing and the flow around the wing. In the opening stage, the thrust coefficient C_T shows a negative value for both the

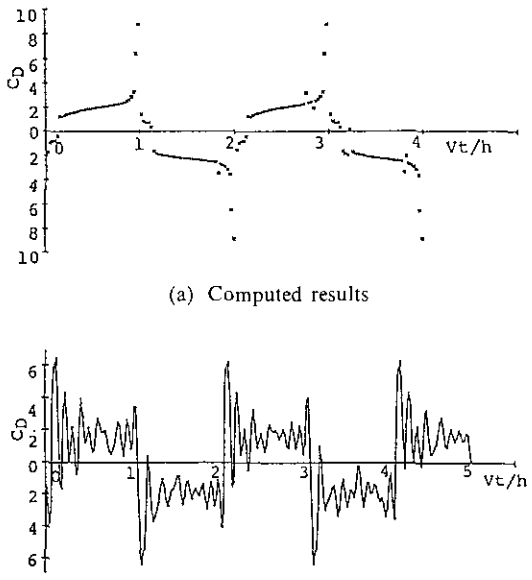

(a) Computed results

(b) Measured results

Fig. 8 Time variations for drag coefficients($C=1$, $h=4C$, $V/U=1.0$, $r_p=0.75C$, $\alpha=30°$)

calculated and measured results while in the translating stage, the calculated results show an increase as time passes. This trend is not analyzable from the empirical results in the early phases of this stage due to severe fluctuation. However, after the middle phase of the stage, when the fluctuation has stabilized, an increasing trend of the thrust coefficient with time is noticeable, as is in the calculated value. This trend is even more distinguishable when the high frequency area is filtered through FFT(Fast Fourier Transform) (Tsutahara and Kimura, 1987: and Tsutahara, Kimura and Ro, 1989).

Figure 8 shows the calculated and measured results of the drag coefficient C_D taken in the same conditions as in Fig. 7. The drag coefficient C_D *also showed a fairly good match in the qualitative* trend between the calculated and measured results. However in the closing stage, the calculated values increased rapidly while the measured values didn't show any significant signs of increase. This might be due to the fact that in the analytical model of Fig. 2, the wing was approximated as a flat-plate airfoil of no thickness and the flow surrounding the wing was assumed as 2-dimensional. In the actual experiment, the speci-

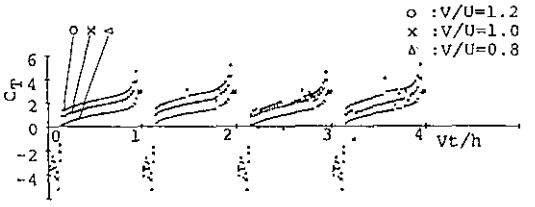

(a) Thrust coefficient

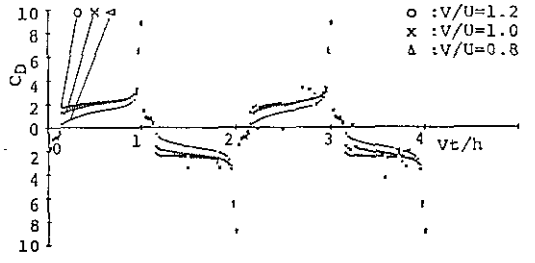

(b) Drag coefficient

Fig. 9 Thrust and drag coefficients for the velocity ratio($\alpha=30°$)

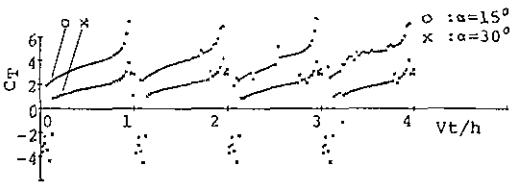

(a) Thrust coefficient

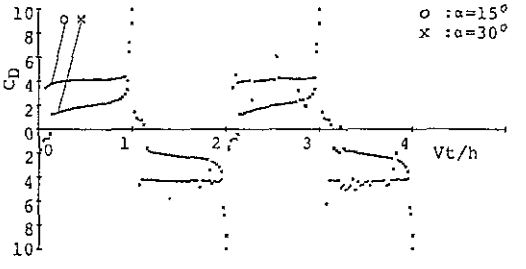

(b) Drag coefficient

Fig. 10 Thrust and drag coefficients for the opening angle($V/U=1.0$)

men was shaped in a complete winglike form having thickness. Also, the water surface above the wing would affect the flow around the wing making it not thoroughly 2-dimensional. When we compare the calculation results from Figs. 7 and 8, the thrust coefficient does not increase in the closing stage, but the drag coefficient does very rapidly. Generally, the efficiency is defined as the ratio of output C_TU to the given input C_DV, but in this case, because the velocity ratio V/U=1.0, the efficiency of the closing stage is lower than the efficiency of the translating stage. This implies that the jet flow generated between the wing and the channel surface during the closing stage, explained in the last journal(Ro, 1993), does not contribute to the increase in efficiency.

Figure 9 shows when $\alpha=30°$, the calculated results of the thrust coefficient C_T and the drag coefficients C_D throughout the 4 strokes for different values of the velocity ratio V/U. In a stroke of the wing motion, the thrust coefficient shows the same pattern regardless of the change in velocity ratio. However the drag coefficient increases dramatically as the part having the smaller velocity ratio moves closer to the channel surface. This implies that the drag coefficient is more seriously affected by the channel surface with decreasing the velocity ratio. Meanwhile, in the translating stage, both the mean value of the thrust and drag coefficients increase along with the velocity ratio.

Figure 10 shows the calculated results of the thrust coefficient C_T and the drag coefficient C_D when the open angle $\alpha=15°$, 30° and the velocity ratio V/U=1.0. In general, the thrust and drag coefficients have a higher value when $\alpha=15°$ than $\alpha=30°$. In the translating stage, the thrust coefficient increases at both angles when the wing moves closer to the channel surface. In comparison, the drag coefficient would increase when the angle was 30° but remained steady when the angle was 15°. This meant that in the case of the drag coefficient, it would be more affected by the channel surface as the open angle would increase.

5. Conclusion

The time history of the thrust and drag coefficient of the ship propulsion mechanism of Weis-Fogh type was discussed by the discrete vortex method. The unsteady components of the force and moment acting on the wing were calculated as the argument difference between the upper and lower surfaces of the wing, in consideration of the

strength changes of the bound vortices representing the wing surface area. The results of the calculations are coincided with the empirical results and the dynamic characteristics of the propulsion mechanism can be stated as follows.

(1) The thrust coefficient and drag coefficients increase proportionally with velocity ratio.

(2) The jet flow created in the closing stage hardly contribute to the increase in efficiency.

(3) Assuming identical conditions, the thrust and drag coefficients when the open angle $\alpha=15°$ are higher than when the angle is 30°.

(4) In the translating stage, the drag coefficient is the more influenced by the channel surface when the velocity ratio is smaller or when the open angle is larger.

To add to the conclusion, this study has proven that the discrete vortex method is very effective in calculating the complex flow field in situations where the object moves unsteadily or when there is unsteadily separated flow.

References

Edwards, R. H. and Cheng, H. K., 1982, "The Separation Vortex in the Weis-Fogh Circulation-Generation Mechanism," *Journal of Fluid Mechanics*, Vol. 120, pp. 463~473.

Furber, S. B. and Ffowcs Williams, J. E., 1979, "Is the Weis-Fogh Principle Exploitable in Turbomachinary ?," *Journal of Fluid Mechanics*, Vol. 94, Part 3, pp. 519~540.

Maxworthy, T., 1979, "Experiments on the Weis-Fogh Mechanism of Lift Generation by Insects in Hovering Flight. Part 1. Dynamics of the 'Fling'," *Journal of Fluid Mechanics*, Vol. 93, pp. 47~63.

Lighthill, M. J., 1973, "On the Weis-Fogh Mechanism of Lift Generation," *Journal of Fluid Mechanics*, Vol. 60, Part 1, pp. 1~17.

Ro, K. D. and Tsutahara, M., 1997-3, "Numerical Analysis of Unsteady Flow in the Weis-Fogh Mechanism by the 3D Discrete Vortex Method with GRAPE3A, " *Transactions of the ASME, Journal of Fluids Engineering*, Vol. 119, pp. 96~102.

Ro, K. D., 1993, "Development of the Weis-Fogh Type Ship Propulsion Mechanism (Visualization and Numerical Analysis of the Flow Field)," *Transactions of the KSME*, Vol. 17, No. 2, pp. 426~437 in Korean.

Spedding, G. R. and Maxworthy, T., 1986, " The Generation of Circulation and Lift in a Rigid Two-Dimensional Fling," *Journal of Fluid Mechanics*, Vol. 165, pp. 247~272.

Tsutahara, M. and Kimura, T., 1987, "An Application of the Weis-Fogh Mechanism to Ship Propulsion," *Transactions of the ASME, Journal of Fluids Engineering*, Vol. 109, pp. 107~113.

Tsutahara, M., Kimura, T. and Ro, K. D., 1989, "Ship Propulsion Using the Weis-Fogh Mechanism," *Bulletin of the Marine Engr. Soc. in Japan*, Vol. 17, No. 2, pp. 49~55.

Tsutahara, M. and Kimura, T., 1987, "A Pilot Pump Using the Weis-Fogh Mechanism and its Characteristics," *Transactions of the JSME*, Vol. 54, No. 498, pp. 393~397.

Tsutahara, M. and Kimura, T., 1994, "Study of a Fan Using the Weis-Fogh Mechanism (An Experimental Fan and its Characteristics)," *Transactions of the JSME*, Vol. 60, No. 571, pp. 910~915.

Tsutahara, M., Kimura, T. and Ro, K. D., 1989, "Unsteady Pressure and Force in the Discrete Vortex Methods," *Transactions of the Japan Soc. Aero. Space Sci.* Vol. 32, No. 97, pp. 129~142.

Weis-Fogh, T., 1973, "Quick Estimates of Flight Fitness in Hovering Animals, Including Novel Mechanism for Lift Production, " *Journal of Experimental Biology*, Vol. 59, pp. 169~230.